Structural basis for CD1d presentation of a sulfatide derived from myelin and its implications for autoimmunity

Dirk M. Zajonc,[1] Igor Maricic,[4] Douglass Wu,[2,3] Ramesh Halder,[4] Keshab Roy,[4] Chi-Huey Wong,[2,3] Vipin Kumar,[4] and Ian A. Wilson[1,3]

[1]Department of Molecular Biology, [2]Department of Chemistry, and the [3]Skaggs Institute for Chemical Biology, The Scripps Research Institute, La Jolla, CA 92037
[4]Torrey Pines Institute for Molecular Studies, San Diego, CA 92121

Sulfatide derived from the myelin stimulates a distinct population of CD1d-restricted natural killer T (NKT) cells. Cis-tetracosenoyl sulfatide is one of the immunodominant species in myelin as identified by proliferation, cytokine secretion, and CD1d tetramer staining. The crystal structure of mouse CD1d in complex with cis-tetracosenoyl sulfatide at 1.9 Å resolution reveals that the longer cis-tetracosenoyl fatty acid chain fully occupies the A′ pocket of the CD1d binding groove, whereas the sphingosine chain fills up the F′ pocket. A precise hydrogen bond network in the center of the binding groove orients and positions the ceramide backbone for insertion of the lipid tails in their respective pockets. The 3′-sulfated galactose headgroup is highly exposed for presentation to the T cell receptor and projects up and away from the binding pocket due to its β linkage, compared with the more intimate binding of the α-glactosyl ceramide headgroup to CD1d. These structure and binding data on sulfatide presentation by CD1d have important implications for the design of therapeutics that target T cells reactive for myelin glycolipids in autoimmune diseases of the central nervous system.

CORRESPONDENCE
Ian A. Wilson:
wilson@scripps.edu
OR
Vipin Kumar:
vkumar@tpims.org

Abbreviations used: α-GalCer, α-galactosyl ceramide; CNS, central nervous system; EAE, experimental autoimmune encephalomyelitis; Endo H, Endoglycosidase H; iGB3, isoglobotrihexosyl ceramide; MS, multiple sclerosis; NKT, natural killer T; PC, phosphatidyl choline; SF9, *Spodoptera frugiperda*.

Innate pathways of immunity are important not only in providing a rapid response against infectious agents, but also in the effective induction and/or modulation of adaptive responses. Natural killer T (NKT) cells that share the cell-surface receptors of NK cells and, in addition, express an antigen receptor (TCR) are generally stimulated by lipid antigens and rapidly secrete large amounts of IFN-γ and IL-4 after activation (1). NKT cells influence the outcome of the immune response against tumors and infectious organisms, as well as the course of several autoimmune diseases (2, 3).

NKT cells recognize lipid antigens when bound by nonpolymorphic, MHC class I–like CD1 molecules (4). APCs, such as dendritic cells, macrophages, and subsets of B cells, express CD1 molecules. The CD1 family consists of five distinct genes (CD1a–e) that can be categorized into two groups. In humans, group 1 consists of CD1a, CD1b, CD1c, and CD1e, whereas CD1d is the only member of group two and is also expressed in mice.

The first crystal structure of mouse CD1d revealed a deep hydrophobic ligand binding groove, which seems to be well-suited for the binding of long chain hydrophobic compounds, such as lipids, where electron density for two long aliphatic chains was observed, but not fully interpreted, in the binding groove (5). Recently, this bound self-ligand was identified as phosphatidyl choline (PC), and the CD1d crystal structure confirmed that the two lipid tails are inserted into the A′ and F′ pockets, with the headgroup extending out of the groove for T cell recognition (6).

Other structural determinations of a variety of CD1–ligand complex structures, such as CD1a–sulfatide (7), CD1a–lipopeptide (8), CD1b–phosphatidyl inositol, and CD1b–GM2 (9), CD1b–glucose monomycolate (10), mouse CD1d–α-galactosyl ceramide (α-GalCer; short-chain, C_8; reference 11), and human CD1d–α-GalCer (long-chain, C_{26}; reference 12), have provided fascinating insights into the general mode of ligand binding and elucidated the basis for CD1 isotype-specific variation. Each lipid ligand inserts its aliphatic moieties, either two alkyl chains for glycolipids or one alkyl chain for lipopeptides, into the deeply buried hydro-

The Journal of Experimental Medicine

phobic cavities of CD1, thereby positioning the diverse T cell epitopes, carbohydrate moieties for glycolipids and peptidic moieties for lipopeptides, above the hydrophobic binding groove on the CD1 surface for inspection by TCRs specific for either the ligand and/or the CD1 isoform (13).

Because different lipids are either present in or traffic to distinct endocytic compartments, it has been suggested that the different CD1 isotypes have evolved to target these various intracellular locations. CD1b and CD1d are localized mainly in the late endosomes or lysosomes where microbial lipids accumulate after infection, whereas CD1a recycles back to the cell surface via passage through early or recycling endosomes (14, 15). Recently, a family of endosomal lipid transfer proteins, the saposins, has been shown to be necessary for the presentation of certain lipids by CD1. It has been proposed that these saposins have the ability to extract and bind monomeric lipids from the membrane, which could then be transferred through a yet unknown mechanism to CD1 in the endosomal compartments (16–18).

Characterization of lipid-reactive NKT cells and their function is important for understanding the role of this NKT cell subset in the spectrum of immune responses. NKT cells have regulatory effects in both experimental models and in human autoimmune diseases, such as diabetes and multiple sclerosis (2, 3). These cells are autoreactive and express a memory/activation phenotype. NKT cells are heterogeneous, but most of their phenotypic and functional characteristics have been derived from studies of the major mouse NKT cell population that expresses TCRs with an invariant $V\alpha14^+$ α-chain ($V\alpha24^+$ in human). A nonmammalian glycolipid, α-GalCer, has been invaluable as a highly potent, stimulatory ligand for these NKT cells in the context of CD1d. α-GalCer, unlike most mammalian glycolipids, has its carbohydrate moiety attached via an α rather than a β linkage. Thus, very little is known about the phenotype or physiological relevance of self-glycolipid–reactive NKT cells compared with the α-GalCer–reactive invariant NKT cells.

Recently, self-lipids have been identified as ligands for both invariant (i) and variant CD1d-restricted NKT cells (19–21). Although iNKT cells recognize isoglobotrihexosyl ceramide (iGB3), a distinct CD1d-restricted population recognizes sulfatide when presented by CD1d (19, 20). Staining of cells with sulfatide–CD1d–tetrameric complexes ex vivo demonstrated that sulfatide-reactive NKT cells are present in the liver, thymus, and spleen. Interestingly, during the normal course of experimental autoimmune encephalomyelitis (EAE), a prototype model for T cell–mediated autoimmune disease that is characterized by inflammation and demyelination in the central nervous system (CNS), NKT cells reactive against sulfatide–CD1d tetramers, but not α-GalCer–CD1d tetramers, are increased severalfold within the CNS (19). Furthermore, the treatment of mice with 20 mg sulfatide prevents antigen (MOG35-55 peptide)-induced EAE in $CD1d^{+/+}$ mice, but not in $CD1d^{-/-}$ C57BL/6 mice (19). Thus, a sulfatide-reactive subset of NKT cells can be targeted for manipulation of autoimmune responses in experimental autoimmunity.

In an attempt to characterize self-glycolipid recognition by NKT cells and, more precisely, to elucidate the structural differences in ligand binding and NKT cell stimulation between α-anomeric (α-GalCer) versus β-anomeric (sulfatide) glycolipids by mouse CD1d, we crystallized CD1d in complex with a synthetic sulfatide self-antigen and determined its three-dimensional structure at 1.9 Å resolution.

RESULTS

Sulfatide recognition by CD1-restricted T cells

One of the most abundant galactolipids in the axon-insulating myelin sheet of the CNS is 3′ sulfogalactosyl ceramide (sulfatide), in which the 3′ OH of galactose is sulfated and the sugar is attached to the ceramide via a β-glycosidic link-

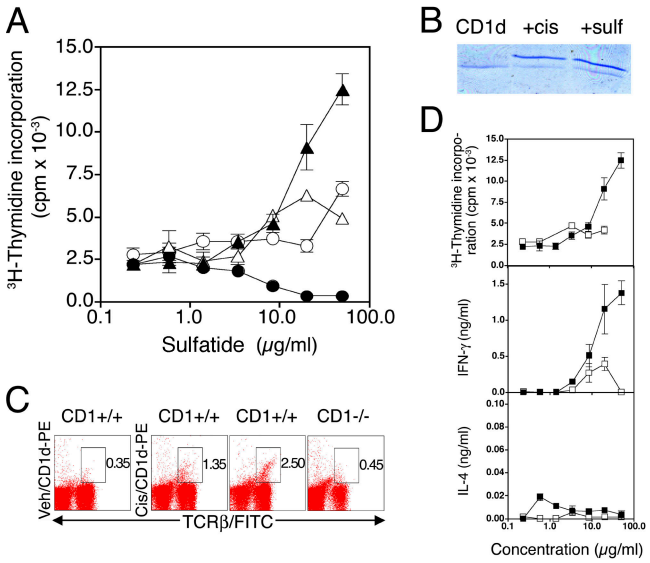

Figure 1. CD1d loading and T cell recognition of sulfatide. (A) Dominant response to cis-tetracosenoyl sulfatide as examined by in vitro proliferation to a titrated dose of cis-tetracosenoyl ($C_{24:1}$) sulfatide (▲), tetracosanoyl ($C_{24:0}$) sulfatide (△), lyso-sulfatide (no fatty acid; ●), and palmitoyl ($C_{16:0}$) sulfatide (○) in splenocytes from C57BL/6 mice. One of three representative experiments is shown. (B) Loading of cis-tetracosenoyl sulfatide onto mouse CD1d molecules. 9 μg of purified mouse CD1d protein was incubated at 37°C for 6 h with 4 μg of purified sulfatide (sulf) from bovine brain or synthetic cis-tetracosenoyl sulfatide (cis) and subjected to IEF gel electrophoresis. One of two representative experiments is shown. (C) Staining of mononuclear cells from liver with cis-tetracosenoyl sulfatide CD1d/tetramer. Flow cytometric analysis of liver mononuclear cells from $CD1d^{+/+}$ (C57BL/6, panels 1 and 2, or SJL/J, panel 3) and C57BL/6.$CD1d^{-/-}$ mice (panel 4) after staining with either cis-tetracosenoyl sulfatide loaded or unloaded CD1d tetramers, which were labeled with phycoerythrin (PE) and anti–TCR-β–FITC. In each panel, the numbers indicate the percent of positive cells. One of three representative experiments is shown. (D) Proliferation and cytokine secretion response of splenocytes from naive C57BL/6 (■) or C57BL/6.$CD1d^{-/-}$ (□) mice to an in vitro stimulation with a titrated dose of cis-tetracosenoyl sulfatide. One of five representative experiments is shown.

age. We have shown that sulfatide is recognized by a subset of CD1d-restricted T cells that are distinct from the invariant $V\alpha14^+$ T cells that respond to the potent glycolipid, α-GalCer, as well as to a sphingolipid self-antigen, iGB3, and the microbial glycuronosyl ceramides (4, 20). Sulfatides derived from the brain are comprised of several molecular species that differ in length of their acyl chain and in the extent of the unsaturation and hydroxylation of the N-amide–linked fatty acid of the ceramide backbone. Thus, natural sulfatide is a 2:1 mixture of saturated and unsaturated fatty acyl chains with tetracosanoyl (C_{24}) constituting the predominant chain length (22).

To analyze the fine specificity of sulfatide-reactive T cells, we have used synthetic homologues or analogs of sulfatide comprised of different fatty acid chain lengths (C_{16}–C_{24}) to characterize the immunodominant sulfatide species. In vitro proliferation or cytokine secretion assays were used to determined the most active species as cis-tetracosenoyl ($C_{24:1}$, mono-unsaturated fatty acid) sulfatide (Fig. 1 A). Other sulfatides, including tetracosanoyl- (C_{24}, saturated fatty acid), palmitoyl- (C_{16}, saturated fatty acid), and lyso-sulfatides (lacking the fatty acid chain) did not induce a significant immune response (Fig. 1 A). Furthermore, adjuvant-free administration of cis-tetracosenoyl sulfatide in three different mouse strains resulted in significant amelioration of a chronic and relapsing form of EAE (unpublished data). Sulfatides, either naturally derived from bovine brain or as synthetic cis-tetracosenoyl species, can be efficiently loaded onto purified mCD1d, as judged by isoelectric focusing gel electrophoresis (Fig. 1 B). The negative charge on the sulfatide promotes a shift in the migration of exogenously loaded mCD1d compared with endogenous CD1d, which is likely loaded with a neutral self-antigen, such as PC (6).

Next, we determined whether synthetic cis-tetracosenoyl sulfatide is able to form mCD1d-tetramers that can stain NKT cells, similar to the recent experiments with tetramers that were loaded with natural sulfatides from bovine brain (19). In two different $CD1d^{+/+}$ mouse strains, around 1–2% of T cells can be stained with cis-tetracosenoyl/mCD1d-tetramers, whereas no staining was observed in $CD1d^{-/-}$ mice or when unloaded tetramers were used to stain NKT cells in a $CD1d^{+/+}$ mouse (Fig. 1 C). To examine the nature of immune response to cis-tetracosenoyl sulfatide and its dependence on the CD1d antigen presentation pathway, spleen cells from naive wild-type mice, as well as $CD1d^{-/-}$ mice, were cultured with different concentrations of the synthetic glycolipid and assayed for proliferation as well as IFN-γ and IL-4 secretion (Fig. 1 D). Splenocytes from wild-type mice, but not from $CD1d^{-/-}$ mice, proliferated and produced IFN-γ in response to cis-tetracosenoyl sulfatide. No significant secretion of IL-4 was observed under these experimental conditions.

The sulfatide negative charge arises from the 3′ sulfate group. Because mono-GM1 that contains sialic acid, which is also negatively charged, does not induce proliferative/cytokine responses, and because GM1–CD1d-tetramers do not stain NKT cells (unpublished data), it seems unlikely that the negative charge alone is responsible for specific recognition by NKT cells. In addition, the 3′ sulfate group is required for the activation of sulfatide-specific NKT cells because β-GalCer, which is identical to the sulfatide but lacks the 3′ sulfate group, does not stimulate this NKT cell pool. As 3′-sulfated α-GalCer is also not able to activate sulfatide-specific NKT cells (unpublished data), it is suggested that these sulfatide-reactive NKT cells are specific for the configuration of the sulfated galactose moiety (β form active, α form inactive) at the CD1d surface.

Table I. Data collection and refinement statistics for the CD1d–sulfatide complex

Data collection	
Resolution range (Å)[a]	50.0–1.9 (1.97–1.9)
Completeness (%)[a]	98.7 (99.7)
Number of unique reflections	67,171
Redundancy	2.4
R_{sym}[a,b] (%)	8.9 (58.0)
I/σ[a]	15.9 (2.4)
Refinement statistics	
Number of reflections ($f>0$)	65,745
Maximum resolution (Å)	1.9
R_{cryst}[c] (%)	18.6 (26.3)
R_{free}[d] (%)	24.8 (33.7)
Number of atoms	6,918
Protein	5,948
Glycolipid ligand	122
N-linked carbohydrate	99
Water	749
Ramachandran statistics (%)	
Favored	98.2
Allowed	1.8
Root-mean-square deviation from ideal geometry	
Bond length (Å)	0.016
Bond angles (°)	1.75
Average B-values (Å²)[e]	
Protein	24.5
Sulfatide (total/ceramide/headgroup/)	42.7/36.5/61.6
Water molecules	34.5
Carbohydrates	37.8

[a]Number in parentheses refer to the highest resolution shell.
[b]$R_{sym} = (\Sigma_h\Sigma_i \mid I_i(h)-<I(h)>I \mid (\Sigma_h\Sigma_i I_i(h))\times 100$, where $<I(h)>$ is the average intensity of i symmetry-related observations for reflections with Bragg index h.
[c]$R_{cryst} = (\Sigma_{hkl} \mid F_o-F_c \mid /\Sigma_{hkl} \mid F_o \mid)\times 100$, where F_o and F_c are the observed and calculated structure factors, respectively, for all data.
[d]R_{free} was calculated as for R_{cryst}, but on 3% of data excluded from refinement.
[e]B-values were calculated with the CCP4 program TLSANL (reference 53).

Structure determination of the CD1d–sulfatide complex

Soluble and fully glycosylated, heterodimeric mouse CD1d-β_2M protein (residues 1–279 heavy chain and 1–99 β_2M) was secreted by *Spodoptera frugiperda* (SF9) cells upon infection with recombinant baculovirus and purified to homogeneity by affinity and size-exclusion chromatography, as described below in Materials and methods. After partial deglycosylation of the protein using Endoglycosidase H (Endo H), synthetic cis-tetracosenoyl sulfatide was loaded by incubating CD1d with a 10-fold molar excess of sulfatide without any detergents. The CD1d–sulfatide complex was further purified by size-exclusion chromatography. More than 95% of the CD1d protein appeared to be loaded with sulfatide, as judged by native IEF gel electrophoresis (unpublished data). Using the sitting drop vapor diffusion method, we crystallized the CD1d–sulfatide complex and determined its three-dimensional structure by molecular replacement using the protein coordinates of the CD1d short-chain α-GalCer complex (PDB code 1Z5L) as the search model (Table I and Fig. 2; reference 11). The crystal structure was refined to a final R_{cryst} and R_{free} of 18.6 and 24.8%, respectively. The asymmetric unit of the crystal contains two CD1d–sulfatide complexes (A and B), which are very similar (root-mean-square deviation of 0.55 Å for all C_α atoms). Thus, we describe here only the crystal structure for complex A, except where stated otherwise.

Structural features of the mouse CD1d–sulfatide complex

The overall architecture of mouse CD1d has been described (5, 6, 11). The binding groove of CD1d is formed by two anti-parallel α-helices that sit atop a six-stranded, β-sheet platform and is lined mainly by hydrophobic residues (Fig. 2 A). The two major pockets, A′ and F′, are located deep inside the CD1 protein and each accommodate one alkyl chain of the sulfatide ligand. The sulfated galactose headgroup is then positioned above the binding groove at the interface between both pockets (Fig. 2 B). As the A′ pocket is larger in volume than the F′ pocket, the synthetic sulfatide (Fig. 2 C, left) binds such that the longer cis-tetracosenoyl fatty acid ($C_{24:1}$) occupies the A′ pocket, whereas the shorter sphingosine backbone (C_{18}) is inserted into the F′ pocket. As the sulfatide alkyl chains then fully occupy both binding pockets, the previously reported spacer lipid (11) is not observed in the CD1d binding groove. Although the electron density is relatively weak at the junction where the cis-tetracosenoyl fatty acid starts to encircle the central pole of the A′ pocket, the fatty acid appears to go around the A′ pole in a counterclockwise direction when looking down into the binding groove (Fig. 3, A and B). This conformation places the cis-unsaturation in the middle of the fatty acid curvature, which could facilitate the encircling of the pole. Several water molecules are located in the vicinity of the polar groups of the sulfatide, mainly proximal to the galactosylsulfate headgroup, which suggests that these waters play a role in the CD1–ligand interaction (Figs. 3 and 4). In contrast, no water molecules could be observed at similar locations in the CD1d short-chain α-GalCer (PBS-25) structure (11), likely due to the closer binding of the α-linked galactose to the α2-helix of CD1d.

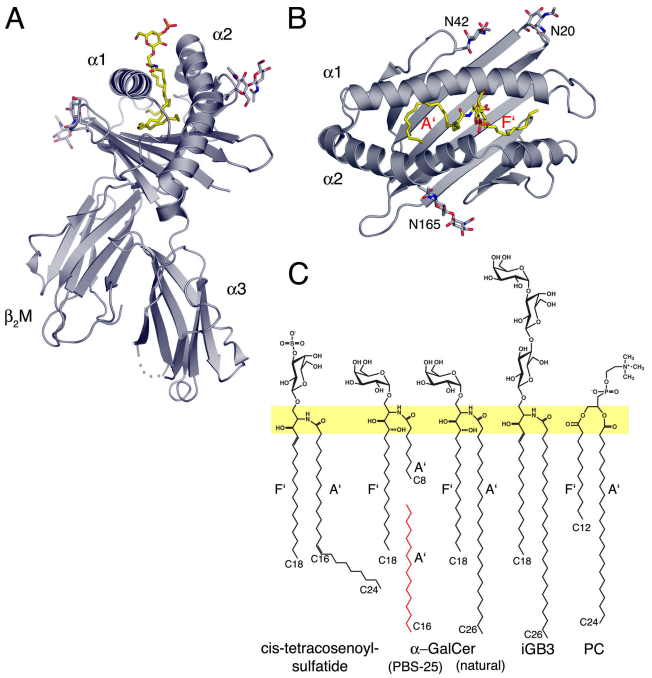

Figure 2. Overview of the CD1d–sulfatide structure. (A) Schematic representation (front view) of the CD1d (α1–α3 domains)-β_2M heterodimer (gray) with β-strands and α-helices highlighted and with bound cis-tetracosenoyl sulfatide ligand in stick representation (yellow). N-linked carbohydrates are depicted as gray stick models. Atom colors for all structural representations are as follows: yellow/gray, carbon; red, oxygen; blue, nitrogen; orange, sulfate. (B) Top view looking into the CD1d-binding groove. The sulfatide fatty acid is bound in the larger A′ pocket, and the sphingosine backbone is bound in the F′ pocket. N20, N42, and N165 represent the three ordered N-linked glycosylation sites that carry at least the remaining proximal N-acetylglucosamine residue after deglycosylation. (C) The chemical structure of the sulfatide used in this study and other CD1d ligands, such as PC (6), iGB3 (20), and the short-chain α-GalCer variant PBS-25 (11) for structural comparison. The length of the individual alkyl chains is given as the number of carbon atoms (C_{12}–C_{26}).

As in the CD1d–PBS-25 structure, the electron density is best defined for the polar region of the sphingosine backbone and the connection with the fatty acid (Fig. 3), as hydrogen bonds with CD1d residues stabilize and provide specificity for this region of the ligand (Fig. 4). Seven hydrogen bonds are formed directly between CD1 and the sulfatide, whereas two additional hydrogen bonds are mediated by water molecules—one between the sulfate group and the backbone nitrogen of Gln154 and the other between the keto group of the fatty acid and the backbone oxygen of Met69. The same CD1 residues are involved in hydrogen bond formation with the short-chain α-GalCer ligand PBS-25. Although several residues of the α1-helix (Asp80, Arg79, and Met69) provide specific contacts to the ceramide back-

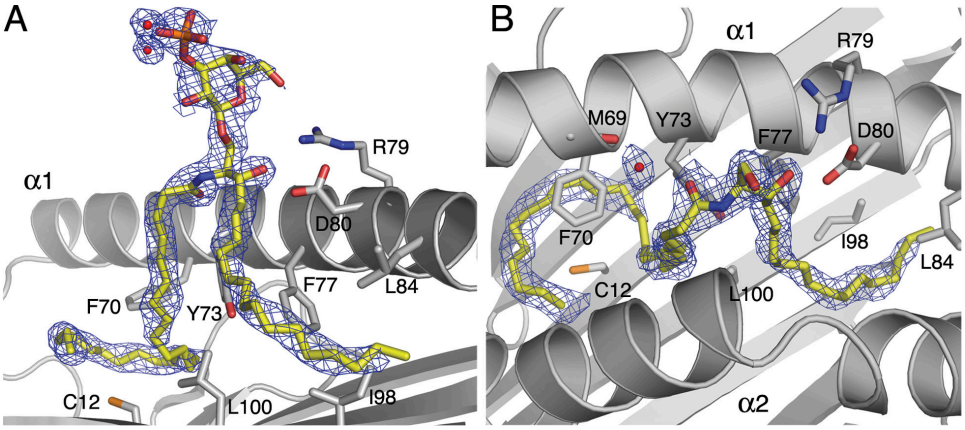

Figure 3. Conformation of the sulfatide in the CD1d-binding groove. After refinement, a $2F_o$-F_c electron density map was calculated and contoured at 1σ as a blue mesh around the ligand (yellow). Several important contact residues that are involved in ligand binding are depicted and labeled. (A) Side view, after removing the α2-helix for clarity. (B) View looking down into the CD1d-binding groove (TCR view). The sulfogalactosyl headgroup is omitted to highlight the well-defined electron density around the branching point of the lipid backbone, which we propose acts as a constraint to orient the different alkyl chains into their specific binding pockets.

bone, the α2-helix (Asp153, Thr156, and Gln154) is more involved in stabilizing the galactosyl headgroup. Nevertheless, Arg79 hydrogen bonds to the 6′ hydroxyl group of the galactose, thereby fixing the orientation of galactose between the α1- and α2-helices in concert with Asp153, which interacts with the 2′ hydroxyl group on the opposite side of the galactose. The sulfate group is only loosely bound, which explains its high B-values (∼70Å^2) compared with the rest of the ligand (∼40Å^2) or the surrounding CD1 residues (24–53Å^2).

Although the sulfated galactose headgroup makes an additional hydrogen bond with CD1d, as compared with the short-chain α-GalCer variant PBS-25 (11), its electron density is less well-defined. The β-linkage between the galactose and the ceramide backbone in the sulfatide results in a much higher degree of solvent exposure of the headgroup, whereas the two short hydrogen bonds (2.5Å and 2.6Å) between Asp153 and the α-linked galactose of PBS-25 pull the galactose toward the α2-helix in an orientation horizontal to the CD1 surface, which results in more intimate contacts with CD1d, as reflected by similar B-values of the PBS-25 galactose and the surrounding CD1 residues.

Comparison of α- versus β-anomeric ligands

A comparison of the orientation of the sulfatide and the PBS-25 ligand in the mCD1d binding groove (Fig. 5, A and B) illustrates that their lipid backbones are bound in a similar location, likely due to the specific hydrogen bonding between the ceramide moiety and the CD1 residues, whereas the different linkage between the galactose headgroups and the lipid (α vs. β) results in conformational differences between each CD1d–lipid complex. The β-anomeric galactose (sulfatide) is highly exposed and projects out of the binding groove perpendicular to the α1- and α2-helices (Fig. 5 A), whereas the

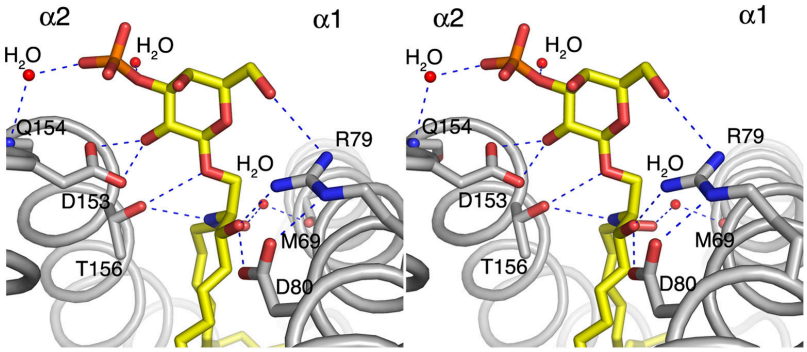

Figure 4. Stereo view of the hydrogen–bond network between sulfatide and CD1d. The sulfatide ligand bound in the CD1d-binding groove is shown in a rear view from the COOH-terminal end of the α1-helix. Hydrogen bonds between the protein and the ligand residues are depicted as blue dashed lines and range in distance from 2.5Å to 3.5Å. The α1-helix residues Arg79 (R79), Asp80 (D80), and Met69 (M69) mainly bind the lipid backbone, whereas Asp153 (D153), Thr156 (T156), and Gln154 (Q154) of the α2-helix interact more closely with the galactose headgroup.

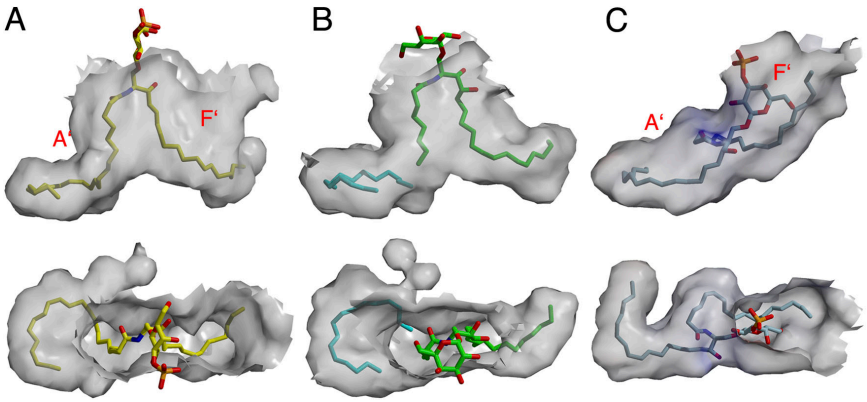

Figure 5. Comparative binding analysis of different CD1d ligands. The CD1d binding pocket is shown as a transparent molecular surface in a side view (top) or top view (bottom), either with (A) bound cis-teracosenoyl sulfatide ($C_{24:1}$) or with (B) the short-chain α-GalCer variant PBS-25 (PDB code 1Z5L). Although the galactose of sulfatide presented by CD1d is more exposed and sticks out from the center of the groove, that of PBS-25 sits more closely above the CD1d surface while burying the lipid backbone underneath. (C) The stearoyl sulfatide ($C_{18:0}$) ligand is more nestled in the CD1a-binding groove (PDB code 1ONQ), whereas the fatty acid tail end is exposed at the CD1 surface.

α-anomeric galactose (PBS-25) sits flat atop the binding groove between both helices, thereby burying the lipid backbone while simultaneously exposing less surface area for recognition by the semi-invariant Vα14 NKT cell receptor (Fig. 5 A and B, bottom). However, the short-chain α-GalCer ligand PBS-25 induces the formation of a roof above the F′ pocket (Fig. 5 B) from CD1d residues, which can now play a role in CD1d–TCR interaction. Small chemical differences in the structure and binding of CD1d-specific ligands can then be directly transmitted to the CD1d surface and, therefore, can aid in ligand discrimination by NKT cells. In the case of the sulfatide ligand, where the galactosylsulfate moiety sticks out of the groove, interaction with the variant sulfatide-reactive NKT cells is likely to be different from iNKT cells. Here, the TCR has to accommodate a more protruding headgroup and a different conformation of residues on the CD1d surface. In addition, the sulfatide ligand exposes more of its lipid backbone, which could now play a role in the T cell–recognition process and help explain the biological differences among various sulfatide species that have different length fatty acid chains (Fig. 1 A).

Comparison of sulfatide binding by CD1d and CD1a

To compare the binding of sulfatides to different CD1 isotypes, the mouse CD1d–sulfatide (Fig. 5 A) complex was analyzed against the previously determined CD1a–sulfatide structure (Fig. 5 C; reference 7). In both cases, the β-linked galactose moieties face upward and are either sandwiched between both α-helices (CD1a) or 90° rotated, sitting above the binding groove (mCD1d). In each case, the sulfate is the most exposed group of the ligand and the major antigenic epitope, as sulfate-lacking β-GalCer is not antigenic (unpublished data). Interestingly, the sulfate ligand is inserted into the two CD1 binding grooves in opposite orientations. In CD1a, the sphingosine backbone occupies the fixed-size A′ pocket (C_{18}, molecular ruler), and the fatty acid tail end extends out of the F′ pocket (C_{18}) at the CD1 surface. In mCD1d, the A′ pocket is much larger and fully accommodates the longer fatty acid chain (C_{24}), whereas the sphingosine backbone now occupies the smaller F′ pocket. In either case, the more restricted of the two CD1 binding pockets binds the fixed-length sphingosine chain, whereas the larger (CD1d) or more open-ended (CD1a) pockets bind the more variable fatty acid. Thus, two different modes of sulfatide binding are found in these CD1 isoforms. In CD1a, the binding groove is fully occupied by the ligand, and any variation in the length of the fatty acid can be accommodated by extension outside the binding groove, which can then directly translate into possible direct contact with the TCR. In mCD1d, the shorter fatty acid chains result in partial filling of the A′ pocket. Depending on the extent of the A′ pocket that is not occupied by a ligand, a pocket-stabilizing factor, as observed for the short-chain α-GalCer variant PBS-25, is then recruited to fill up the unoccupied cavity to form a stable complex (11). In mouse CD1d, the corresponding T cell would not directly see variations in fatty acid chain length at the CD1 surface, whereas for CD1a, these subtle differences in length can directly affect T cell stimulation (23).

DISCUSSION

The CD1 family of glycosylated cell-surface receptors constantly surveys the lipid content of APCs by intracellular trafficking through the various endosomal compartments. The number and different classes of lipids that are now known to act as ligands at the cell surface of APCs for specific T cells have increased significantly in the last few years and include phosphoglycerolipids, sphingolipids, diacylated glycerolipids, lipopeptides, mycolates, phosphomycoketides, and small hydrophobic compounds (for review see references 13–15). Some of these CD1 ligands promiscuously bind to all CD1 isotypes (e.g., sulfatide), whereas others are isoform-specific. For example, mycolates are only bound to CD1b, whereas

phosphomycoketides bind to CD1c. These observations were at first surprising. Sulfatides and lipopeptides, which have quite different chemical composition, can both bind to CD1a but do so in a way that does not alter the structure of the CD1a-binding groove. Both ligands maneuver into the binding groove and attain an optimal fit without inducing any changes in the CD1 conformation (7, 8). In contrast, structures of mCD1d in complex with either PC, sulfatide, or the short-chain α-GalCer PBS-25 show interesting structural changes at the T cell–recognition surface of CD1. Compared with the first crystal structure of mouse CD1d, to which an endogenous PC ligand was bound (5, 6), binding of the short-chain α-GalCer variant results in an alteration at the CD1 surface, which leads to the formation of a roof above the F′ portal (11). This induced fit, however, has not been observed in the structure of mCD1d–sulfatide. Although both sulfatide and α-GalCer are glycosphingolipids, they differ in their chemical structure, not only in the linkage to their galactosyl headgroups, but also in their ceramide lipid backbone. α-GalCer is based on phytoceramide, which has 3′ and 4′ OH groups, whereas the ceramide of sulfatide has a 4′ OH group and a 4′–5′ unsaturation. This additional 4′ OH group of α-GalCer forms a second hydrogen bond with Asp80, and the α-anomeric galactose forms tight hydrogen bonds with Asp153 of the α2-helix. We propose that this tighter hydrogen bond interaction of α-GalCer with both α-helices results in the structural changes observed in the mouse CD1d–α-GalCer complex. PC is a glycerolipid and its lipid backbone diacylglycerol, as well as the phosphorylcholine headgroup, interestingly form fewer hydrogen bonds with CD1 and, therefore, do not appear to induce any structural changes, although no truly "empty" structure is known. However, the crystal structure of human CD1d with bound full-length α-GalCer shows that under certain experimental conditions, such as refolding without ligands, the protein can undergo structural changes that partially close the binding groove. Two CD1d molecules were observed in the crystal structure: one was loaded with α-GalCer, whereas the other was empty. However, whether this capacity of human CD1d to close the binding groove in absence of any detectable ligand is biologically significant remains elusive. Under physiological conditions, such as during folding in the ER, lipids are always present to stabilize the hydrophobic CD1d binding groove, thereby rendering any requirement for gross structural changes unnecessary.

All of the four lipid ligands that have been crystallized in complex with either human (12) or mouse (6, 11) CD1d so far show a common mode of lipid binding. The C_{18} sphingosine chain is always inserted in the F′ pocket, and fatty acid (C_8–C_{26}) is always inserted in the A′ pocket. This orientation is similar for PC, where the shorter fatty acid chain (C_{12}) is inserted in the A′ pocket and the longer fatty acid (C_{24}) in the F′ pocket. Nevertheless, a sphingolipid with a C_{18} fatty acid, as found in sulfatides from natural sources, could insert its two alkyl chains in either pocket if the length of the alkyl chain is the only factor responsible for ligand binding. But the crystal structure of the CD1d–α-GalCer (PBS-25) complex revealed that the short fatty acid (C_8) is surprisingly inserted only in the A′ pocket. The orientation still needs to be determined for the recently identified family of α-anomeric microbial ligands, the glycuronosyl ceramides (C_{14}; references 24 and 25). Thus, we propose that the N-amide linkage between the fatty acid and the sphingosine together with the hydroxyl groups of the sphingosine chain (Fig. 2 C, highlighted in yellow), which forms a precise hydrogen-bonding network with CD1, constrains the ceramide backbone that orients the respective tails into the A′ and F′ pockets.

It is not known whether the immunodominance of cis-tetracosenoyl sulfatide is due to a more efficient binding to CD1d or to the presence of specific TCR repertoires that are stimulated preferentially by individual sulfatide species. In this regard, it is interesting to note that the T cell hybridoma specific for lyso-sulfatide does not recognize any of the other sulfatides examined so far (unpublished data). Whether NKT cells specific for each individual sulfatide express a unique TCR or whether overlapping TCR repertoires exist is currently not clear and should be determined by generating T cell hybridomas reactive to each of the individual sulfatides. Of interest, however, is that although the hydrogen bonding network formed between the lipid backbone and CD1d is responsible for the orientation of the different lipid ligands in the binding groove, slight differences in the positioning of sulfatide and α-GalCer can be observed when both structures are superimposed (not depicted). The same is true when the binding of α-GalCer to CD1d is compared in both mouse and human crystal structures. The exchange of one residue at the CD1d surface (Trp153 in human and Gly155 in mouse) results in a different positioning of the galactose, whereas the lipid backbone is bound in the same orientation (26). Therefore, it is possible that the biological differences between the different sulfatide species shown in Fig. 1 A are not only the result of differential loading characteristics of the ligands, but rather the consequence of subtle structural differences upon ligand binding due to either differences in fatty acid chain length and/or saturation (C_{16} vs. $C_{24:1}$), or, in case of lyso-sulfatide, the complete lack of a fatty acid chain. However, it cannot be completely ruled out that the stronger NKT cell activation by cis-tetracosenoyl sulfatide is a result of the increased solubility of the monounsaturated and more polar nervonyl ($C_{24:1}$) fatty acid versus the fully saturated tetracosanoyl ($C_{24:0}$) fatty acid, which could lead to an increased efficiency of loading onto CD1.

Recognition of sulfatide by CD1d-restricted NKT cells has important implications in autoimmune diseases of the CNS, as sulfatides are one of the major glycolipid components of the myelin membranes that are targeted in such diseases as multiple sclerosis (MS). MS is a demyelinating disease mediated by a T cell–guided immune response that is either initiated from antigen-presenting events in the CNS

or induced after the peripheral activation by a systemic molecular mimicry response (27, 28). Indeed, in MS patients, increased serum levels of glycolipids (29, 30) and antibodies directed against them have been reported (31–34). T cells specific for glycolipids have been isolated from MS patients. Their frequency in five active MS patients was three times higher compared with five normal individuals (35). Recently, it has been demonstrated that sulfatide binds promiscuously to all of the CD1a, CD1b, CD1c, and CD1d isoforms (36). Because CD1 molecules are up-regulated on macrophages in areas of demyelination in chronic-active MS lesions but not in silent lesions in the brain (37), it is possible that self-glycolipids from myelin could be presented during local inflammation to T cells. Microglia, as well as infiltrating macrophages, could either engulf myelin components or internalize them by Fc receptors or by complement receptor–mediated phagocytosis after binding to myelin-specific antibodies. Thus, activated APCs in the CNS could not only present peptides (MHC) to T cells, but also glycolipids (CD1). Thus, myelin glycolipid–reactive T cells could potentially influence the inflammation and demyelination in the CNS. It is clear from our data (19 and unpublished data) that the peripheral activation of sulfatide-reactive T cells after adjuvant-free administration of sulfatide ameliorates experimental autoimmune disease of the CNS. Because CD1 molecules, unlike the classical MHC molecules, are nonpolymorphic, insight into the molecular recognition of sulfatide by the CD1d molecules and their interaction with a unique CD1d-restricted NKT cell population will be extremely valuable in the potential development of non-HLA–dependent therapeutic approaches for autoimmune demyelinating diseases in humans.

MATERIALS AND METHODS

Mice. 6–8-week-old female C57BL/6 or SJL/J ($CD1d^{+/+}$) mice were purchased from The Jackson Laboratory. C57BL/6 ($CD1d^{-/-}$) mice were originally generated in the laboratory of L. Van Kaer (Vanderbilt University, Nashville, TN) and were provided by M. Kronenberg (La Jolla Institute of Allergy and Immunology, La Jolla, CA). All animals were housed under specific pathogen-free conditions, and animal protocols were approved by the Institutional Animal Care and Use Committee of the Torrey Pines Institute for Molecular Studies.

Reagents. Purified sulfatides from bovine myelin and other semi-synthetic sulfatides, including lyso-sulfatide, palmitoyl-sulfatide, and tetracosanoyl-sulfatide, were purchased from Matreya Inc. Synthetic cis-tetracosenoyl sulfatide was synthesized as reported previously (38). For biological experiments, lipids were dissolved in vehicle (0.5% Tween 20 and 0.9% NaCl solution) and diluted in PBS. For structural studies, cis-teracosenoyl sulfatide was dissolved in DMSO. All monoclonal antibodies were purchased from BD Biosciences.

Cell preparation. Hepatic lymphocytes were isolated using established Percoll gradient methods. In brief, animals were killed by CO_2 inhalation and perfused with chilled PBS. To obtain lymphocytes, the liver was removed, cut into small pieces, passed through a 70-μm nylon cell strainer (Falcon; Becton Dickinson), and suspended in DMEM supplemented with 2% heat-inactivated FBS. After centrifugation (1,500 *g* for 10 min), the cell pellet was washed and resuspended in the same medium. Lymphocytes were isolated from parenchymal hepatocytes, nuclei, and Kupffer cells by Percoll (35% Percoll containing 100 U/ml heparin) gradient separation. Splenocytes were obtained by passing the spleen through a 70-μm nylon strainer and suspension in DMEM with 2% heat-inactivated FBS. Erythrocytes were lysed with RBC lysis buffer (BD Biosciences).

Monoclonal antibodies and flow cytometry. Mononuclear cells were isolated and suspended in FACS buffer ($1–2 \times 10^6$/ml) containing 0.02% NaN_3 in PBS (wt/vol) and 2% FBS (vol/vol) and treated with antibodies against FcR-γ (2.4G2) to block nonspecific binding and then labeled with the indicated monoclonal antibodies. For flow cytometry staining, 2.5 μg of tetramerized mCD1d was used. Flow cytometric analysis was performed on a FACSCalibur instrument using CELLQuest software (Becton Dickinson).

Tetrameric mCD1d–lipid complexes. Mouse CD1d protein was generated using the baculovirus expression system essentially as described previously (19). Unloaded mCD1d tetramers were prepared by preincubating biotinylated mCD1d protein with vehicle only. To produce glycolipid–mCD1d tetramers, biotinylated mCD1d protein was incubated with sulfatide at a molar ratio of 1:6 for 18–20 h at 22°C.

Measurement of proliferative and cytokine responses. For proliferative response to the self-glycolipids, 8×10^5 splenocytes from naive C57BL/6 ($CD1d^{+/+}$) or $CD1d^{-/-}$ mice were cultured in vitro for 72 h in the presence of increasing concentrations of cis-tetracosenoyl sulfatide (5–50 μg/ml). [^{3}H]thymidine incorporation was quantitated as described previously (19, 39). For cytokine secretion, supernatants from 48-h cultures were collected and IFN-γ and IL-4 levels were determined using typical sandwich ELISA assays using reagents from BD Biosciences as described previously (19, 39). IL-2 secretion by sulfatide-reactive NKT cell hybridomas was determined in culture supernatants by standard ELISA.

In vitro loading of sulfatides onto mouse CD1d. Soluble mouse CD1d (9 μg/18 μl in PBS) was mixed with 4 μg (2.0 μl) of purified bovine brain–derived sulfatide or the synthetic cis-tetracosenoyl sulfatide and incubated at 37°C for 6 h followed by washing with 500 μl of PBS and concentrated using 10 kD mol wt cut-off centrifugal concentrators (Millipore). After adjusting the remaining volume, equal amounts of protein were subjected to IEF gel electrophoresis to monitor the loading efficiency of sulfatide onto CD1d.

Protein expression, purification, and crystallization. The baculovirus transfer vector pAcUW51 (BD Biosciences) containing the nucleic acid sequence for the extracellular domains of mCD1d and β_2M, including signal sequence, was provided by M. Kronenberg. To engineer a CD1d construct for crystallization purposes, the biotinylation domain, generally used for the preparation of CD1 tetramers followed by a hexahistidine tag, was removed by digestion with the restriction enzyme BamHI and replaced with a short hexahistidine tag that was introduced by ligation of two complementary BamHI-restricted oligonucleotides. A SalI site was incorporated in the oligonucleotide to verify the integration of the fragment by restriction digestion. Three colonies were analyzed by sequencing to find one clone with the right orientation of the hexahistidine tag. The constructed plasmid was cotransfected into SF9 cells with BaculoGold DNA using Cellfectin reagent (Invitrogen) according to the manufacturer's specifications. After several rounds of virus amplification, the protein was expressed for 3 d in shaking flasks (145 rpm) at 28°C using SF9 cells (2×10^6 cells/ml) with a multiplicity of infection of ~3. The expression experiment was typically performed on a 5–8-liter scale. SF9 cells were removed from the cell culture media by centrifugation, and the media was further concentrated to 1 liter and washed several times with PBS buffer. The protein was purified from the concentrated media by ion metal affinity chromatography on a Ni-NTA resin (QIAGEN) in 50 mM Tris/HCl buffer, pH 8.0, followed by anion-exchange chromatography using MonoQ HR 10/10 (GE Healthcare) in 10 mM Tris/HCl buffer, pH 8.0, with a linear gradient of 0–250

mM NaCl. Two of the four total N-linked carbohydrates were removed after the proximal N-acetyl glucosamine residue by Endo H cleavage, as judged by mass spectrometry analysis (unpublished data). In brief, 1 mg CD1d protein was incubated with 50 mU Endo H in 100 mM sodium acetate, pH 5.9, at 37°C for 2 h and purified by size-exclusion chromatography (Superdex S200 10/300 GL; GE Healthcare). The synthetic sulfatide ligand was then loaded onto the partially deglycosylated protein by incubating 3 mg CD1d with a 10-fold molar excess of synthetic sulfatide (0.12 ml of a 5 mg/ml solution in DMSO) in 100 mM sodium acetate buffer, pH 5.9, for 6 h at 37°C with intermittent agitation. The loaded CD1d protein was purified by ion-exchange chromatography on a MonoQ column using a shallow gradient of NaCl (0–150 mM over 25 column volumes). Loading of sulfatide onto CD1d was observed by native IEF gels that monitored a shift toward the cathode due to the additional negative charge from the sulfate moiety. The CD1d fractions from the MonoQ run were pooled and concentrated to 7.5 mg/ml in 10 mM Hepes, pH 7.5, and 25 mM NaCl. The best crystals were obtained at 22°C by mixing 1 μl protein (7.5 mg/ml) with 1 μl precipitant solution (2 M ammonium sulfate, 0.1 M sodium cacodylate, pH 6.5, 0.2 M NaCl, and 10 mM manganese chloride) and grown for 2 wk for data collection.

Structure determination. Crystals were flash-cooled at a temperature of 100 K in mother liquor containing 25% glycerol. Diffraction data from a single crystal was collected at Beamline 8.2.2 of the Advanced Light Source, Berkeley, CA, and then later from another crystal at Beamline 11.1 of the Stanford Synchrotron Radiation Laboratory and processed to 2.7 Å and 1.9 Å, respectively, with the Denzo-Scalepack suite (40) in spacegroup P2 (unit cell dimensions: $a = 58.86$ Å, $b = 74.84$ Å, $c = 101.56$ Å, and $\beta = 102.1°$). Two CD1–lipid complexes occupy the asymmetric unit with an estimated solvent content of 53.8% based on a Matthews' coefficient (V_m) of 2.66 A^3/Da. Molecular replacement in $P2_1$ was performed with the lower resolution dataset in CCP4 (41) using the program MOLREP (42) and the CD1d-PBS-25 structure (15ZL) as the search model, with the ligand removed, which resulted in a R_{cryst} of 48.2% and a correlation coefficient of 0.46. Subsequent rigid-body refinement in REFMAC 5.2 to a resolution of 3.5 Å resulted in an R_{cryst} of 41.4%. The initial refinement included several rounds of restrained refinement against the maximum likelihood target in REFMAC 5.2. Tight restraints were maintained between the two molecules in the asymmetric unit throughout the refinement of the lower resolution dataset. At a later stage of refinement, carbohydrates were built at 5 out of the 8 N-linked glycosylation sites in both CD1 molecules. When the 1.9 Å high resolution dataset became available, it was then used for subsequent refinement of the model derived from the 2.7 Å resolution data. Before model building and restrained refinement, one round of rigid-body refinement was performed to 3.5 Å resolution that resulted in an R_{cryst} of 28%. Tight noncrystallographic symmetry restraints were applied only during the first round of refinement and then not used further, as they resulted in an increase in the R_{free} value. The refinement progress was judged by monitoring the R_{free} for cross-validation (43). The model was rebuilt into σ_A-weighted $2Fo–Fc$ and $Fo–Fc$ difference electron density maps using the program O (44). Water molecules were assigned during refinement in REFMAC using the water ARP module for $>3\sigma$ peaks in an $Fo–Fc$ map and retained if they satisfied hydrogen-bonding criteria and returned $2Fo–Fc$ density $>1\sigma$ after refinement. Starting coordinates for the sulfatide ligand were obtained from the CD1a–sulfatide structure (1ONQ) and modified accordingly using the molecular modeling system INSIGHT II (Accelrys, Inc.). The sulfatide library for REFMAC (45) was created using the Dundee PRODRG2 server (46). Final refinement steps were performed using the translation, libration, and screw-rotation displacement procedure in REFMAC (47) with a total of six anisotropic domains (three per complex: α1-α2 domain, α3-domain, and β_2M) and resulted in improved electron density maps for the glycolipid ligand and a further drop in R_{free}. The CD1d–sulfatide structure has a final R_{cryst} of 18.6% and an R_{free} of 24.8%. The quality of the model (Table I) was assessed with the program Molprobity (48).

Structure presentation. The program Pymol (49) was used to prepare Figs. 2, 3, and 4. The programs Molscript (50), GRASP (51), and Raster3D (52) were used to prepare Fig. 5.

Accession codes. Coordinates and structure factors for the CD1d–sulfatide complex have been deposited in the Protein Data Bank under accession code 2AKR.

We thank the staffs of the Advanced Light Source, BL 8.2.2, and Stanford Synchrotron Radiation Laboratory BL 11.1 for support with data collection, Julie Vanhnasy for technical assistance, and Petra Verdino, Konstantinos Beis, and James Stevens for helpful discussions.

This study was supported by National Institutes of Health grants GM62116, CA58896 (both to I.A. Wilson), and CA10066 (to V. Kumar), and The Skaggs Institute for Chemical Biology (to I.A. Wilson, C.-H. Wong, and D.M. Zajonc). This is manuscript number 17631-MB of The Scripps Research Institute.

The authors have no conflicting financial interests.

Submitted: 11 August 2005
Accepted: 27 October 2005

REFERENCES

1. Bendelac, A. 1995. Mouse NK1$^+$ T cells. *Curr. Opin. Immunol.* 7:367–374.
2. Godfrey, D.I., and M. Kronenberg. 2004. Going both ways: immune regulation via CD1d-dependent NKT cells. *J. Clin. Invest.* 114:1379–1388.
3. Wilson, S.B., and T.L. Delovitch. 2003. Janus-like role of regulatory iNKT cells in autoimmune disease and tumour immunity. *Nat. Rev. Immunol.* 3:211–222.
4. Kawano, T., J. Cui, Y. Koezuka, I. Toura, Y. Kaneko, K. Motoki, H. Ueno, R. Nakagawa, H. Sato, E. Kondo, et al. 1997. CD1d-restricted and TCR-mediated activation of vα14 NKT cells by glycosylceramides. *Science.* 278:1626–1629.
5. Zeng, Z., A.R. Castano, B.W. Segelke, E.A. Stura, P.A. Peterson, and I.A. Wilson. 1997. Crystal structure of mouse CD1: an MHC-like fold with a large hydrophobic binding groove. *Science.* 277:339–345.
6. Giabbai, B., S. Sidobre, M.D. Crispin, Y. Sanchez-Ruiz, A. Bachi, M. Kronenberg, I.A. Wilson, and M. Degano. 2005. Crystal structure of mouse CD1d bound to the self ligand phosphatidylcholine: a molecular basis for NKT cell activation. *J. Immunol.* 175:977–984.
7. Zajonc, D.M., M.A. Elsliger, L. Teyton, and I.A. Wilson. 2003. Crystal structure of CD1a in complex with a sulfatide self antigen at a resolution of 2.15 Å. *Nat. Immunol.* 4:808–815.
8. Zajonc, D.M., M.D. Crispin, T.A. Bowden, D.C. Young, T.Y. Cheng, J. Hu, C.E. Costello, P.M. Rudd, R.A. Dwek, M.J. Miller, et al. 2005. Molecular mechanism of lipopeptide presentation by CD1a. *Immunity.* 22:209–219.
9. Gadola, S.D., N.R. Zaccai, K. Harlos, D. Shepherd, J.C. Castro-Palomino, G. Ritter, R.R. Schmidt, E.Y. Jones, and V. Cerundolo. 2002. Structure of human CD1b with bound ligands at 2.3 Å, a maze for alkyl chains. *Nat. Immunol.* 3:721–726.
10. Batuwangala, T., D. Shepherd, S.D. Gadola, K.J. Gibson, N.R. Zaccai, A.R. Fersht, G.S. Besra, V. Cerundolo, and E.Y. Jones. 2004. The crystal structure of human CD1b with a bound bacterial glycolipid. *J. Immunol.* 172:2382–2388.
11. Zajonc, D.M., C. Cantu III, J. Mattner, D. Zhou, P.B. Savage, A. Bendelac, I.A. Wilson, and L. Teyton. 2005. Structure and function of a potent agonist for the semi-invariant natural killer T cell receptor. *Nat. Immunol.* 6:810–818.
12. Koch, M., V.S. Stronge, D. Shepherd, S.D. Gadola, B. Mathew, G. Ritter, A.R. Fersht, G.S. Besra, R.R. Schmidt, E.Y. Jones, and V. Cerundolo. 2005. The crystal structure of human CD1d with and without alpha-galactosylceramide. *Nat. Immunol.* 6:819–826.
13. Moody, D.B., D.M. Zajonc, and I.A. Wilson. 2005. Anatomy of CD1-lipid antigen complexes. *Nat. Rev. Immunol.* 5:387–399.
14. De Libero, G., and L. Mori. 2005. Recognition of lipid antigens by T cells. *Nat. Rev. Immunol.* 5:485–496.
15. Brigl, M., and M.B. Brenner. 2004. CD1: antigen presentation and T

cell function. *Annu. Rev. Immunol.* 22:817–890.
16. Zhou, D., C. Cantu III, Y. Sagiv, N. Schrantz, A.B. Kulkarni, X. Qi, D.J. Mahuran, C.R. Morales, G.A. Grabowski, K. Benlagha, et al. 2004. Editing of CD1d-bound lipid antigens by endosomal lipid transfer proteins. *Science.* 303:523–527.
17. Winau, F., V. Schwierzeck, R. Hurwitz, N. Remmel, P.A. Sieling, R.L. Modlin, S.A. Porcelli, V. Brinkmann, M. Sugita, K. Sandhoff, et al. 2004. Saposin C is required for lipid presentation by human CD1b. *Nat. Immunol.* 5:169–174.
18. Kolter, T., and K. Sandhoff. 2005. Principles of lysosomal membrane digestion: stimulation of sphingolipid degradation by sphingolipid activator proteins and anionic lysosomal lipids. *Annu. Rev. Cell Dev. Biol.* 21:81–103.
19. Jahng, A., I. Maricic, C. Aguilera, S. Cardell, R.C. Halder, and V. Kumar. 2004. Prevention of autoimmunity by targeting a distinct, noninvariant CD1d-reactive T cell population reactive to sulfatide. *J. Exp. Med.* 199:947–957.
20. Zhou, D., J. Mattner, C. Cantu III, N. Schrantz, N. Yin, Y. Gao, Y. Sagiv, K. Hudspeth, Y.P. Wu, T. Yamashita, et al. 2004. Lysosomal glycosphingolipid recognition by NKT cells. *Science.* 306:1786–1789.
21. Wu, D.Y., N.H. Segal, S. Sidobre, M. Kronenberg, and P.B. Chapman. 2003. Cross-presentation of disialoganglioside GD3 to natural killer T cells. *J. Exp. Med.* 198:173–181.
22. O'Brien, J.S., D.L. Fillerup, and J.F. Mead. 1964. Quantification and fatty acid and fatty aldehyde composition of ethanolamine, choline, and serine glycerophosphatides in human cerebral grey and white matter. *J. Lipid. Res.* 5:329–338.
23. Compostella, F., L. Franchini, G. De Libero, G. Palmisano, F. Ronchetti, and L. Panza. 2002. CD1a-binding glycosphingolipids stimulating human autoreactive T-cells: synthesis of a family of sulfatides differing in the acyl chain moiety. *Tetrahedron.* 58:8703–8708.
24. Mattner, J., K.L. Debord, N. Ismail, R.D. Goff, C. Cantu III, D. Zhou, P. Saint-Mezard, V. Wang, Y. Gao, N. Yin, et al. 2005. Exogenous and endogenous glycolipid antigens activate NKT cells during microbial infections. *Nature.* 434:525–529.
25. Kinjo, Y., D. Wu, G. Kim, G.W. Xing, M.A. Poles, D.D. Ho, M. Tsuji, K. Kawahara, C.H. Wong, and M. Kronenberg. 2005. Recognition of bacterial glycosphingolipids by natural killer T cells. *Nature.* 434:520–525.
26. Godfrey, D.I., J. McCluskey, and J. Rossjohn. 2005. CD1d antigen presentation: treats for NKT cells. *Nat. Immunol.* 6:754–756.
27. Prat, A., and J. Antel. 2005. Pathogenesis of multiple sclerosis. *Curr. Opin. Neurol.* 18:225–230.
28. Sospedra, M., and R. Martin. 2005. Immunology of multiple sclerosis. *Annu. Rev. Immunol.* 23:683–747.
29. Lubetzki, C., Y. Thuillier, A. Galli, O. Lyon-Caen, F. Lhermitte, and B. Zalc. 1989. Galactosylceramide: a reliable serum index of demyelination in multiple sclerosis. *Ann. Neurol.* 26:407–409.
30. Sela, B.A., G. Konat, and H. Offner. 1982. Elevated ganglioside concentration in serum and peripheral blood lymphocytes from multiple sclerosis patients in remission. *J. Neurol. Sci.* 54:143–148.
31. Uhlig, H., and R. Dernick. 1989. Monoclonal autoantibodies derived from multiple sclerosis patients and control persons and their reactivities with antigens of the central nervous system. *Autoimmunity.* 5:87–99.
32. Stevens, A., M. Weller, and H. Wietholter. 1992. CSF and serum ganglioside antibody patterns in MS. *Acta Neurol. Scand.* 86:485–489.
33. Acarin, N., J. Rio, A.L. Fernandez, M. Tintore, I. Duran, I. Galan, and X. Montalban. 1996. Different antiganglioside antibody patterns between relapsing-remitting and progressive multiple sclerosis. *Acta Neurol. Scand.* 93:99–103.
34. Bansal, A.S., B. Abdul-Karim, R.A. Malik, P. Goulding, R.S. Pumphrey, A.J. Boulton, P.L. Holt, and P.B. Wilson. 1994. IgM ganglioside GM1 antibodies in patients with autoimmune disease or neuropathy, and controls. *J. Clin. Pathol.* 47:300–302.
35. Shamshiev, A., A. Donda, I. Carena, L. Mori, L. Kappos, and G. De Libero. 1999. Self glycolipids as T-cell autoantigens. *Eur. J. Immunol.* 29:1667–1675.
36. Shamshiev, A., H.J. Gober, A. Donda, Z. Mazorra, L. Mori, and G. De Libero. 2002. Presentation of the same glycolipid by different CD1 molecules. *J. Exp. Med.* 195:1013–1021.
37. Battistini, L., F.R. Fischer, C.S. Raine, and C.F. Brosnan. 1996. CD1b is expressed in multiple sclerosis lesions. *J. Neuroimmunol.* 67:145–151.
38. Wu, D., G.W. Xing, M.A. Poles, A. Horowitz, Y. Kinjo, B. Sullivan, V. Bodmer-Narkevitch, O. Plettenburg, M. Kronenberg, M. Tsuji, et al. 2005. Bacterial glycolipids and analogs as antigens for CD1d-restricted NKT cells. *Proc. Natl. Acad. Sci. USA.* 102:1351–1356.
39. Jahng, A.W., I. Maricic, B. Pedersen, N. Burdin, O. Naidenko, M. Kronenberg, Y. Koezuka, and V. Kumar. 2001. Activation of natural killer T cells potentiates or prevents experimental autoimmune encephalomyelitis. *J. Exp. Med.* 194:1789–1799.
40. Otwinowski, Z., and W. Minor. 1997. HKL: processing of X-ray diffraction data collected in oscillation mode. *Methods Enzymol.* 276:307–326.
41. Collaborative Computer Project, Number 4. 1994. The CCP4 suite: programs for protein crystallography. *Acta Crystallogr. D. Biol. Crystallogr.* 50:760–763.
42. Vagin, A.A., and A. Teplyakov. 1997. MOLREP: an automated program for molecular replacement. *J. Appl. Cryst.* 30:1022–1025.
43. Brünger, A.T. 1992. Free R value: a novel statistical quantity for assessing the accuracy of crystal structures. *Nature.* 355:472–475.
44. Jones, T.A., J.Y. Zou, S.W. Cowan, and M. Kjeldgaard. 1991. Improved methods for building protein models in electron density maps and the location of errors in these models. *Acta Crystallogr. A.* 47:110–119.
45. Murshudov, G.N., A.A. Vagin, and E.J. Dodson. 1997. Refinement of macromolecular structures by the maximum likelihood method. *Acta Crystallogr. D.* 53:240–255.
46. Schuettelkopf, A.W., and D.M. van Aalten. 2004. PRODRG: a tool for high-throughput crystallography of protein-ligand complexes. *Acta Crystallogr.D.* 60:1355–1363.
47. Winn, M.D., M.N. Isupov, and G.N. Murshudov. 2001. Use of TLS parameters to model anisotropic displacements in macromolecular refinement. *Acta Crystallogr.D.* 57:122–133.
48. Lovell, S.C., I.W. Davis, W.B. Arendall III, P.I. de Bakker, J.M. Word, M.G. Prisant, J.S. Richardson, and D.C. Richardson. 2003. Structure validation by Cα geometry: ϕ, ψ and Cβ deviation. *Proteins.* 50:437–450.
49. DeLano, W. 2002. The PyMOL Molecular Graphics System. http://www.pymol.org.
50. Kraulis, P.J. 1991. MOLSCRIPT: a program to produce both detailed and schematic plots of protein structures. *J. Appl. Cryst.* 24:946–950.
51. Nicholls, A., K.A. Sharp, and B. Honig. 1991. Protein folding and association: insights from the interfacial and thermodynamic properties of hydrocarbons. *Proteins.* 11:281–296.
52. Merritt, E.A., and D.J. Bacon. 1997. Raster3D: photorealistic molecular graphics. *Methods Enzymol.* 277:505–524.
53. Howlin, B., A.S. Butler, D.S. Moss, G.W. Harris, and H.P.C. Driessen. 1993. TLSANL: TLS parameter analysis program for segmented anisotropic refinement of macromolecular structures. *J. Appl. Cryst.* 26:622–624.